crystals

MDPI

Article

Structure, Electrical Properties, and Thermal Stability of the Mn/Nb Co-Doped Aurivillius-Type $Na_{0.5}Bi_{4.5}Ti_4O_{15}$ High Temperature Piezoelectric Ceramics

Tianlong Zhao, Kefei Shi, Chunlong Fei *, Xinhao Sun, Yi Quan *, Wen Liu, Juan Zhang and Xianying Dai

Key Laboratory of Ministry of Education for Wide Band-Gap Semiconductor Materials and Devices, School of Microelectronics, Xidian University, Xi'an 710071, China

* Correspondence: clfei@xidian.edu.cn (C.F.); quanyi@xidian.edu.cn (Y.Q.)

Abstract: In order to meet the urgent need for high temperature piezoelectric materials with a Curie temperature over 400 °C, the Mn/Nb co-doped strategy has been proposed to improve the weak piezoelectric performance of the Aurivillius-type $Na_{0.5}Bi_{4.5}Ti_4O_{15}$ (NBT) high temperature piezoelectric ceramics. In this paper, the crystal structure, electrical properties, and thermal stability of the B-site Mn/Nb co-doped $Na_{0.5}Bi_{4.5}Ti_{4-x}(Mn_{1/3}Nb_{2/3})_xO_{15}$ (NBT-100x) ceramics were systematically investigated by the conventional solid-state reaction method. The crystal structural analysis results indicate that the NBT-100x ceramics have typical bismuth oxide layer type phase structure and high anisotropic plate-like morphology. The lattice parameters and the grain sizes increase with the *B*-site Mn/Nb co-doped content. The electrical properties were significantly improved by Mn/Nb co-doped modifications. The maximum of the piezoelectric coefficient d_{33} was found to be 29 pC/N for the NBT-2 ceramics, nearly twice that of the unmodified NBT ceramics. The highest values of the planar electromechanical coupling factor k_p and thickness electromechanical coupling factor k_t were also obtained for the NBT-2 ceramics, at 5.4% and 31.2%, respectively. The dielectric spectroscopy showed that the Curie temperature Tc of the Mn/Nb co-doped NBT-100x ceramics is slightly higher than that of unmodified NBT ceramics (646 °C). The DC resistivity of the NBT-2 ceramics is higher than 10^6 Ω·cm at 500 °C. All the results together with the good thermal stability demonstrated the Mn/Nb co-doped ceramics as an effective method to improve the NBT based piezoelectric ceramics and the potential candidates of the Mn/Nb co-doped NBT-100x ceramics for high temperature piezoelectric applications.

Keywords: high temperature piezoelectric; $Na_{0.5}Bi_{4.5}Ti_4O_{15}$; co-doped; thermal stability

Citation: Zhao, T.; Shi, K.; Fei, C.; Sun, X.; Quan, Y.; Liu, W.; Zhang, J.; Dai, X. Structure, Electrical Properties, and Thermal Stability of the Mn/Nb Co-Doped Aurivillius-Type $Na_{0.5}Bi_{4.5}Ti_4O_{15}$ High Temperature Piezoelectric Ceramics. *Crystals* **2023**, *13*, 433. https://doi.org/10.3390/cryst13030433

Academic Editor: Francisco M. Morales

Received: 6 January 2023
Revised: 28 February 2023
Accepted: 1 March 2023
Published: 2 March 2023

1. Introduction

Piezoelectric materials can directly realize the conversion between electrical energy and mechanical energy [1]. They have been widely used in machinery manufacturing, electronic communications, the military, and other fields. Piezoelectric materials played an irreplaceable role in the functional conversion device of force, heat, light, electricity, and magnetism fields and showed a broad application prospect [2–4]. Piezoelectric materials can be divided into crystal, ceramic, polymer, and composite materials [5]. Among all these piezoelectric materials, piezoelectric ceramics have been °Ccupying most of the market share of piezoelectric materials owning to their excellent piezoelectric properties, abundance in component regulation, relatively simple fabrication process, and low cost.

Recently, the operating environment of piezoelectric materials received serious challenges due to the rapid development in the automotive industry, energy industry, aerospace industry, etc [5–7]. For example, the automobile internal combustion engine system required the piezoelectric materials to be able to work steadily under an environment temperature of 200 °C or even 300 °C; the pressure sensor for the detection of hydraulic parameters in the process of oil exploration also presents a new challenge to piezoelectric materials;

and the engine vibration testing in the aerospace field also requires piezoelectric materials to work at higher temperatures. Research on high-temperature piezoelectric materials and their device applications has received unprecedented concern and attention. However, the most commonly used commercial piezoelectric materials, $Pb(Zr,Ti)O_3$ (abbreviated as PZT) ceramics, present a Curie temperature ~ 360 °C due to their composition and structure [1]. For bulk piezoelectric materials, the proper functioning temperature is limited to half the Tc because of the depolarization effect caused by thermal activation, so that the traditional PZT piezoelectric ceramics cannot be used over 200 °C [6]. Therefore, there is an urgent need to search for piezoelectric materials with a Curie temperature of 400 °C or higher.

Aurivillius-type ferroelectrics or bismuth layer structured ferroelectrics (BLSFs) have attracted immense attention for piezoelectric devices operating at high temperatures due to their low dielectric permittivity, high Curie temperature over 400 °C, excellent thermal stability, and strong anisotropic electromechanical properties [8–10]. The general crystal structure of BLSFs can be described as the pseudo-perovskite blocks $(A_{m-1}B_mO_{3m+1})^{2-}$ sandwiched between $(Bi_2O_2)^{2+}$ layers with the formula of $(Bi_2O_2)^{2+}(A_{m-1}B_mO_{3m+1})^{2-}$, where A refers to mono-,bi-, or trivalent ion (e.g., Na^+, K^+, Ca^{2+}, Sr^{2+}, Ba^{2+}, and Bi^{3+}) and B represents a tetra-, penta-, or hexavalent ion (e.g., Ti^{4+}, Nb^{5+}, Ta^{5+}, Mo^{6+} and W^{6+}) [11,12]. This special stacking structure limits the ferroelectric polarization rotation to the a–b plane of the pseudo-perovskite layers. In addition, the electrical properties are sensitively related to the number of BO_6 °Ctahedra m (generally 1–6) due to the ferroelectric polarization derived from the rotation of the BO_6 °Ctahedra [5]. However, this two-dimensional polarization orientation restriction also results in the weak piezoelectric performance of BLSF ceramics.

In order to overcome these shortcomings, great effort has been paid to the lattice structure regulation technology by A-site, B-site, and A-B site composite substitution [13–20]. In these studies, though the A-site modification performs more effectively in the enhancement of the ferroelectric and piezoelectric properties than the B-site modification, the Curie temperature of the BLSFs ceramics after the A-site modification will reduce a lot. For example, the A-site NaBi composite substitution of the $CaBi_2Nb_2O_9$ ceramics led to the Tc decreasing from 925 °C to 880 °C [13]. Recently, it has been proven that B-site multi-ions co-doping is an effective strategy to improve the piezoelectricity of BLSF ceramics [19]. For example, the Mn/Nb co-doped $CaBi_4Ti_4O_{15}$ (CBT) [20] ceramics present an enhanced piezoelectric coefficient of d_{33} 23 pC/N, increasing by 2 times compared with that of the unmodified $CaBi_4Ti_4O_{15}$. Further, a remarkable d_{33} of 24 pC/N was obtained for the Mn/Ta co-doped $CaBi_4Ti_4O_{15}$, with an improved resistivity of 4.96×10^8 Ω·cm at 400 °C [21]. The W/Cr co-substitution at the B-site of $Bi_4Ti_3O_{12}$ (BIT) ceramics presents an enhanced piezoelectric coefficient of d_{33} 31 pC/N together with a Tc of 651 °C [22].

Aurivillius-type sodium bismuth titanate, $Na_{0.5}Bi_{4.5}Ti_4O_{15}$ (NBT), as one of the important members in the BLSFs with m = 4, increasingly arouses the interest of researchers because of its potential in high temperature piezoelectric sensor applications because of its strong ferroelectric polarization and high Curie temperature (Tc ~650 °C) [23]. Unfortunately, the piezoelectricity of unmodified NBT ceramic is very low (d_{33} < 16 pC/N). Since the similar crystalline structure to CBT and BIT, one can expect that the Mn/Nb co-doped modification strategy may also be suitable for the electrical property optimization of NBT. In this paper, the effects of the B-site Mn/Nb co-doped on the structure and electrical properties of NBT ceramics were investigated, and the relevant physical mechanisms were discussed in detail.

2. Experimental Methods

2.1. Fabrication

Samples of the Aurivillius-type $Na_{0.5}Bi_{4.5}Ti_{4-x}(Mn_{1/3}Nb_{2/3})O_{15}$ (NBT-100x, x = 0.00, 0.01, 0.02, 0.03, and 0.04, respectively) ceramics were synthesized by the conventional solid-state reaction methods using the raw materials Na_2CO_3 (99.8%), Bi_2O_3 (99.8%), TiO_2 (99.9%), MnO_2 (99.9%), and Nb_2O_5 (99.5%). The detailed process flow diagram is shown in Figure 1. All the analytical-grade raw materials were selected and weighed according

to the formulation designed above, and then the mixture was ball-milled in an alcohol medium for 12 h. After pre-fired synthesis at 800–850 °C for 3 h, the above mixture was subsequently ball-milled and dry-compressed into pellets of 12 mm in diameter and 1.5 mm in thickness. After burning out the glue of PVA at 600 °C for 12 h, the disks were sintered at 1050–1150 °C for 3 h and buried with the same composition powders. The final samples of the NBT-100x were polished to a thickness of about 0.8 mm before the structural analysis and electrical measurements.

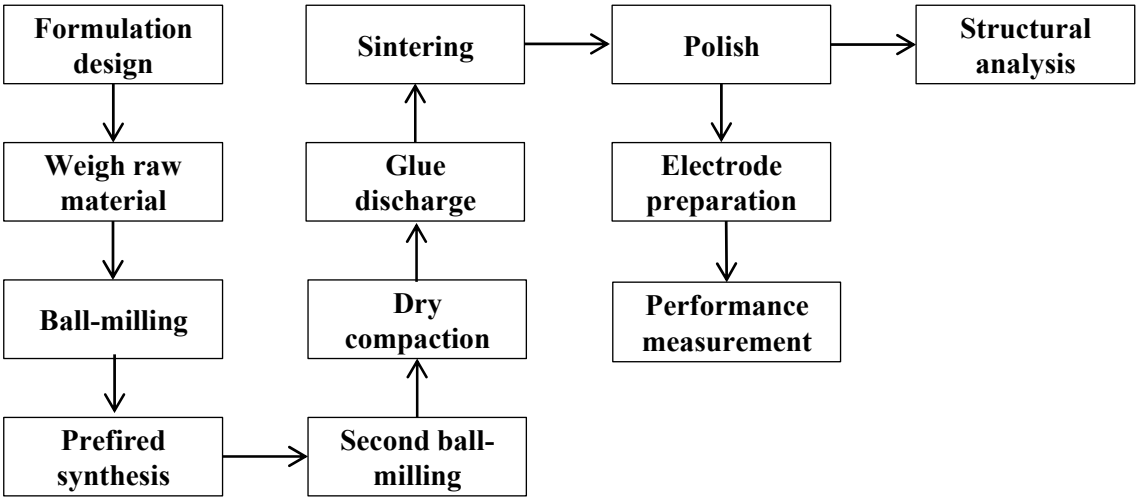

Figure 1. Process flow diagram of the NBT-100x piezoelectric ceramics.

2.2. Characterization

The crystal structure, electrical properties, and thermal stability of the B-site Mn/Nb co-doped Aurivillius-type $Na_{0.5}Bi_{4.5}Ti_{4-x}(Mn_{1/3}Nb_{2/3})O_{15}$ (NBT-100x) high temperature piezoelectric ceramics were systematically investigated. For the crystal structural analysis, we selected X-ray diffraction (XRD) technology to characterize the phase structure and lattice parameter using Cu Kα (D8 Advance, Bruker AXS GmbH, Billerica, MA, USA), and scanning electron microscopy (SEM) technology to observe the surface microstructure with the equipment (S-4800, Hitachi, Tokyo, Japan). Before the electrical measurements, the ceramic samples were poled by a DC electric field of 10 kV/mm for 20 min in a 180 °C silicone oil medium, and then the performance measurements were conducted according to the IEEE standards [24]. For the dielectric property measurements, we selected the impedance analyzer (Agilent, 4294A, Santa Clara, CA, USA) to obtain the dielectric permittivity ε and the dielectric loss tan δ in the frequency range of 1 kHz to 1 MHz from room temperature to 700 °C. For the piezoelectric property measurements, we selected the quasi-static Berlincourt meter (ZJ-3A, Ningbo, China) to obtain the piezoelectric coefficient d_{33} and the impedance analyzer (Agilent 4294A, USA) to obtain the electromechanical coupling performance by the resonance–antiresonance method. For the thermal stability measurements, we selected the digit multimeter (Model 34410A $6\frac{1}{2}$, Agilent) to obtain the DC resistivity from room temperature to 700 °C. However, the effects of thermal depoling on piezoelectric performance were investigated by annealing the ceramic samples at each temperature range from 100 °C to 650 °C for 1 h and subsequently measuring the piezoelectric coefficient d_{33} after cooling down to room temperature.

3. Results and Discussions

Figure 2 shows the X-ray diffraction results of the Mn/Nb co-doped NBT ceramics, which indicate a typical bismuth oxide layer type structure. The strongest diffraction peak is found to be the (119) diffraction peak for all the samples, in accordance with the previous report that the most intense reflections are (11$2m$ + 1) types for the Aurivillius-type ferroelectrics [12]. In addition, a secondary phase of the $Bi_4Ti_3O_{12}$ (117) can be detected for

all the samples near the diffraction angle $2\theta = 30°$, which is a common phenomenon in the BLFS [25]. It can be observed that the peaks for Mn/Nb co-doped NBT ceramics shift to the lower angle region with the increase of Mn/Nb contents x, indicating a slight crystal lattice distortion with the introduction of Mn/Nb compound ions into the NBT ceramics. This trend is clearly shown in Figure 2b for the (119) diffraction peak.

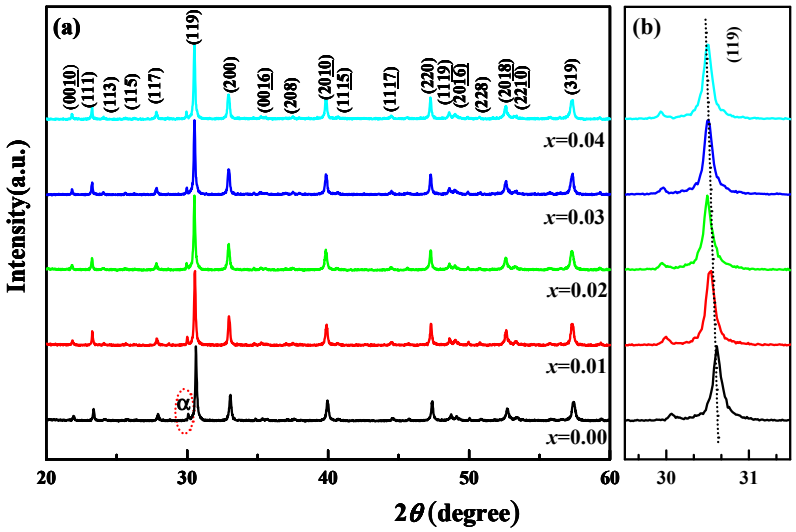

Figure 2. Room temperature X-ray diffraction patterns of the Mn/Nb co-doped NBT ceramics. (**a**) From bottom to top, Mn/Nb content 0.00, 0.01, 0.02, 0.03 and 0.04 respectively. Note: Additional peaks α: $Bi_4Ti_3O_{12}$ (117). (**b**) Selected (119) diffraction peak shift to the lower angle.

The diffraction peaks shifting to a lower angle region indicate an increasing lattice parameter according to the Bragg diffraction formula. To certify this point, the lattice parameters of the Mn/Nb co-doped NBT ceramics were calculated and illustrated in Figure 3. Obviously, all the lattice parameters increase with the doping level x. It can be explained as follows. In this work, the Mn/Nb co-doped NBT ceramics were sintered at 1100 °C, and the Mn ions and Nb ions will be of the types Mn^{2+} and Nb^{5+}, respectively. The multi ions of Mn^{2+} and Nb^{5+} will enter the *B*-site of the NBT ceramics as the equal type of $(Mn_{1/3}Nb_{2/3})^{4+}$. Due to the larger ionic radius of $(Mn_{1/3}Nb_{2/3})^{4+}$ (Mn^{2+} 0.67Å and Nb^{5+} 0.64 Å for CN = 6) than that of Ti^{4+} (0.605Å for CN = 6) [26], the lattice parameters of the *B*-site Mn/Nb co-doped NBT ceramics will increase as a result. Furthermore, a decreasing a/b ratio with the increasing doping level can be identified in Figure 3b, revealing the decreasing anisotropy in the *a*-*b* plane of the Mn/Nb co-doped NBT ceramics.

Figure 4 shows the natural surface SEM images for the Mn/Nb co-doped NBT ceramics sintered at 1100 °C: (a) x = 0.00, (b) x = 0.01, (c) x = 0.02, (d) x = 0.03, and (e) x = 0.04, respectively. There are no obvious porosities that can be seen from the SEM images, indicating the well densified ceramic samples after the sintering process. Similar to other BSLFs materials, the Mn/Nb co-doped NBT ceramics also exhibit the high anisotropy plate-like morphology, with the grains having about 5 to 7 times the length l as the thickness t. This phenomenon may be attributed to the higher grain growth rate along the *a*-*b* plane than that along the *c*-axis plane. In addition, it can be seen that the length l of the plate-like grains increases with the increasing Mn/Nb co-doped content from 0.00 to 0.04. This enlarged grain size can be attributed to the Mn ions, which lower the sintering temperature and facilitate the grain growth as a result.

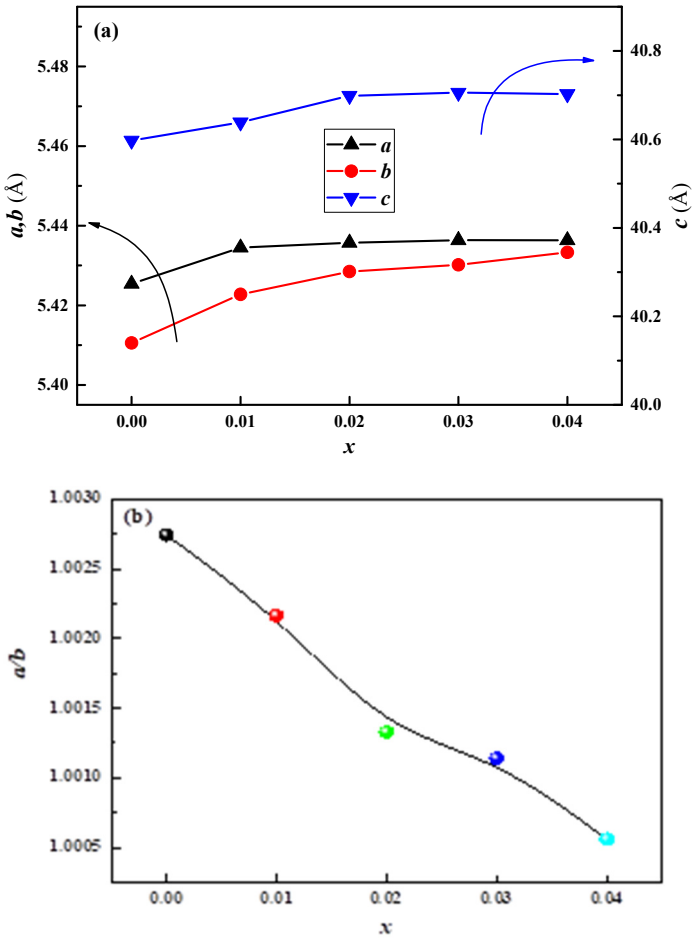

Figure 3. (**a**) Lattice parameters *a*, *b*, and *c*; (**b**) a/b ratio of the Mn/Nb co-doped.

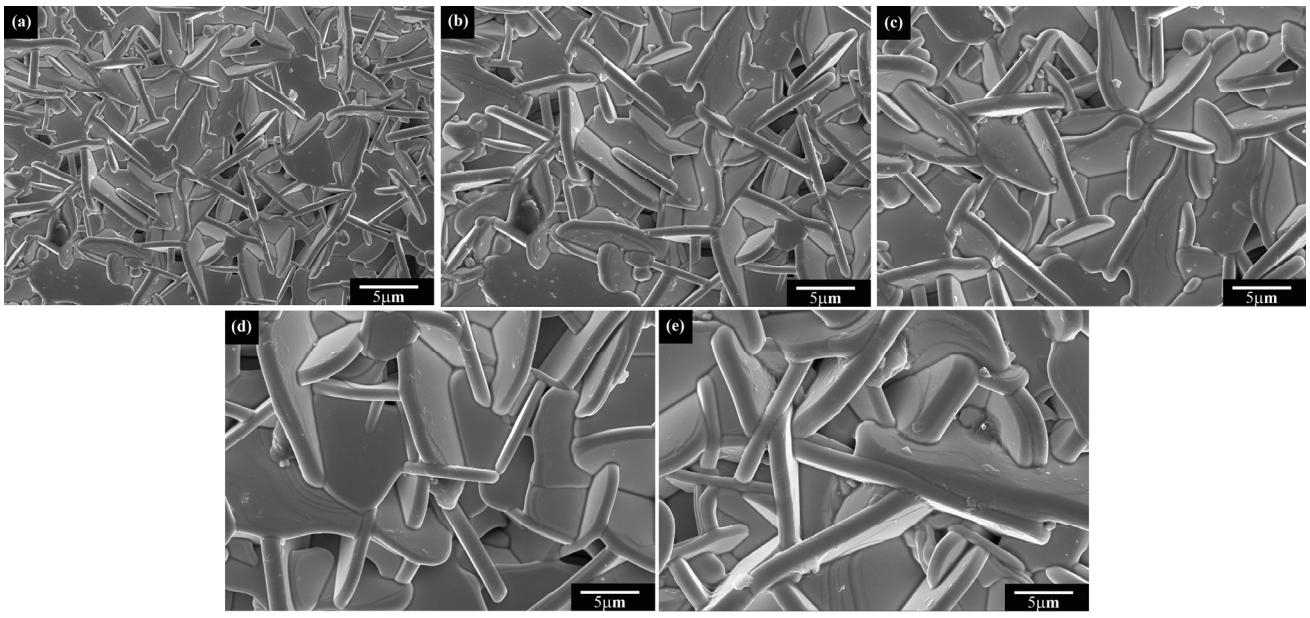

Figure 4. Natural surface SEM images for the Mn/Nb co-doped NBT ceramics sintered at 1100 °C: (**a**) $x = 0.00$, (**b**) $x = 0.01$, (**c**) $x = 0.02$, (**d**) $x = 0.03$, and (**e**) $x = 0.04$.

Figure 5 presents the variation of the room temperature dielectric permittivity ε and the dielectric loss tan δ for the Mn/Nb co-doped NBT ceramics in the frequency range of

1 kHz to 1MHz. The dielectric permittivity decreases a little with no obvious dispersion, and the dielectric loss tan δ is lower than 0.006 in the measured frequency range. In addition, it can be figured out that the Mn/Nb co-doped material has a significant influence on the dielectric properties. With the increasing doping level x, the dielectric permittivity increases from 145 to 160, and the dielectric loss tan δ reduced, especially at 1MHz. The optimized dielectric properties may be attributed to the decreasing anisotropy in the a-b plane caused by Mn/Nb co-doping.

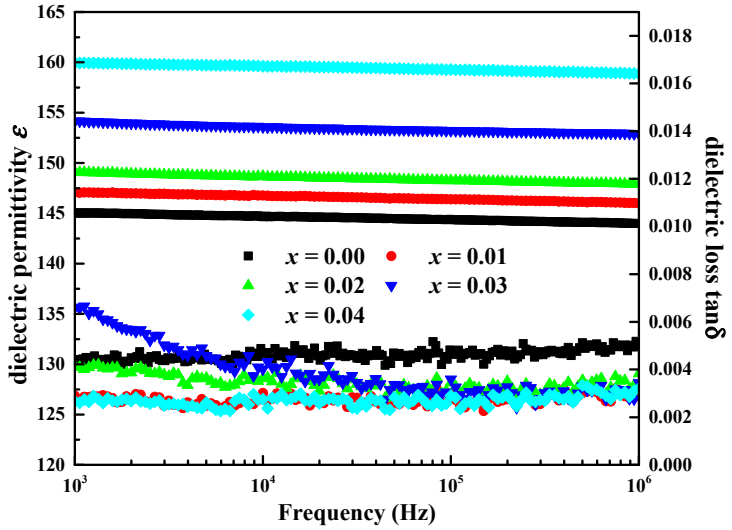

Figure 5. Room temperature dielectric permittivity and dielectric loss tan δ for the Mn/Nb co-doped NBT ceramics as a function of frequency.

Figure 6 shows the temperature dependence of the dielectric permittivity ε and the dielectric loss tan δ at 1MHz for the Mn/Nb co-doped NBT ceramics. It can be clearly seen that a single dielectric peak was detected, which is in accordance with the transition temperature of the ferroelectric phase the paraelectric phase, that is, the Curie temperature (T_c). From the inset, it is obvious that the T_c is sensitive to the Mn/Nb co-doped contents and linearly increases from 646 °C to 660 °C with the increasing doping level x. Generally, the Curie temperature is closely related to the crystal lattice distortion in the pseudo-perovskite blocks $(A_{m\text{-}1}B_mO_{3m+1})^{2-}$ in BLSFs. This distortion can be described by the tolerance factor t given by the next equation [27]:

$$t = \frac{r_A + r_O}{\sqrt{2}(r_B + r_O)}$$

where r_A, r_B, and r_O are the ionic radii of the A-site ion, B-site ion, and oxygen ion in the $(A_{m-1}B_mO_{3m+1})^{2-}$, respectively. Empirically, it presents a higher transition temperature with a smaller tolerance factor t. As discussed before, the larger ion radii Mn^{2+} and Nb^{5+} replace the Ti^{4+} and enter the B-site of the NBT ceramics due to the similar ionic radii (Mn^{2+} 0.67Å, Nb^{5+} 0.64 Å, and Ti^{4+} 0.605Å for CN = 6). Thus, the tolerance factor t reduces due to the enlarged r_B and results in an increase in the Curie temperature. Furthermore, the dielectric loss tan δ of the Mn/Nb co-doped NBT ceramics is lower than 0.05 until the temperature reaches 400 °C, which is important for high temperature piezoelectric applications.

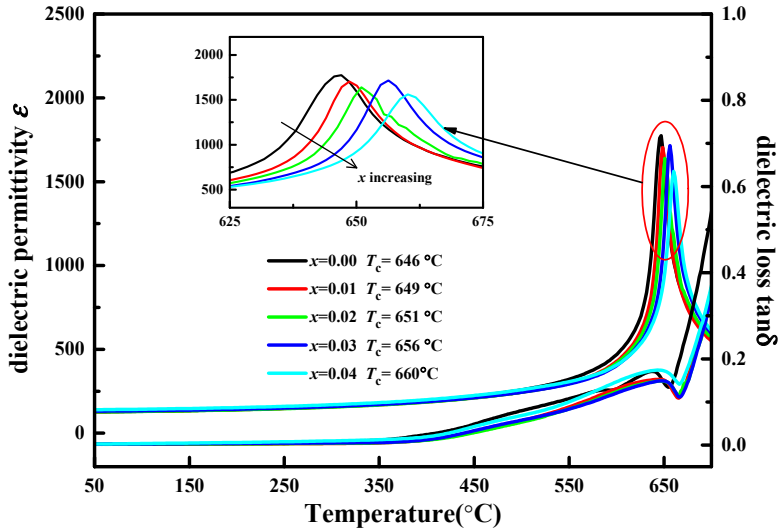

Figure 6. Temperature dependence of dielectric permittivity and dielectric loss tan δ at 1 MHz for the Mn/Nb co-doped NBT ceramics.

The room temperature electrical properties are measured and summarized in Figure 7. It can be seen that the electrical properties of NBT ceramics are significantly improved by Mn/Nb co-doping, and the piezoelectric coefficient d_{33} is sensitive to the Mn/Nb co-doped contents, as well as the electromechanical coupling factor k. The maximum of the d_{33} was found to be 29 pC/N for the NBT-2 ceramics, nearly twice that of the unmodified NBT ceramics. When you compare this improvement in piezoelectric coefficient d_{33} with that of other NBT based ceramics reported in the past two years, such as the Cr_2O_3-modified $Na_{0.5}Bi_{4.5}Ti_4O_{15}$-$Na_{0.5}Bi_{0.5}TiO_3$ composite ceramics 25 pC/N [15], the $Na_{0.5}Bi_{4.5-x}Ce_xTi_4O_{15}$ ceramics 20 pC/N [23], the $Na_{0.5}Bi_{4.46}Ce_{0.04}Ti_{4-x}Co_xO_{15}$ ceramics 22 pC/N [28], the $(Na_{0.5}Bi_{0.5})_{1-x}CaxBi_4Ti_4O_{15}$ ceramics 22 pC/N [29], our finding exhibits an obvious advantage, demonstrating that the Mn/Nb co-doping is an effective method to enhance the piezoelectric properties of the NBT-based piezoelectric. In addition, the highest values of the planar electromechanical coupling factor k_p and the thickness electromechanical coupling factor k_t were also obtained for the NBT-2 ceramics, at 5.4% and 31.2%, respectively, indicating strong anisotropic electromechanical coupling performance due to the two-dimension rotation restriction of the ferroelectric polarization. However, the mechanical quality factor Q_m increased linearly from 4200 to 6020 with the increasing doping level x. As discussed before, the Mn^{2+} and Nb^{5+} substitute for the B-site Ti^{4+} because of the close ionic radii. However, the Mn^{2+} always plays a role in the domain wall pinning in the modification of the piezoelectric ceramics [30,31]. With the increasing Mn/Nb compound ions introduction into the NBT ceramics, the domain wall motion was restricted and the mechanical quality factor Q_m increased.

Figure 8 presents the temperature dependence of the DC resistivity of the NBT and NBT-2 ceramics. It can be found that the DC resistivity is enhanced by the introduction of Mn/Nb compound ions into the NBT ceramics during the measured temperature range. According to the Arrhenius relationship $\rho = \rho_0 \exp(-E_a/kT)$, the activation energies E_a of the NBT and NBT-2 ceramics were calculated and shown in the inset as 1.02 and 1.16 eV, respectively, indicating that the oxygen vacancies dominate the conduction process. This is because the diffusion activation energy of oxygen vacancies in oxide solid solutions is nearly 1 eV. In this work, the enhanced resistivity and activation energy may be attributed to the variable valences of Mn ions. As discussed above, the Mn^{4+} ions may reduce to Mn^{2+} ions in the ceramic sintering process. Then the Mn^{2+} may enter the B-site and replace the Ti^{4+} because of the similar ion radius. The oxygen vacancies, which dominate the conduction process, will generate as a result. Furthermore, the Mn^{2+} ions will enhance the domain wall pinning effect [20] and restrict the movements of the oxygen vacancies,

leading to higher resistivity. In addition, the DC resistivity of the NBT-2 ceramics is higher than 10^6 Ω cm at 500 °C, showing potential for high temperature piezoelectric applications.

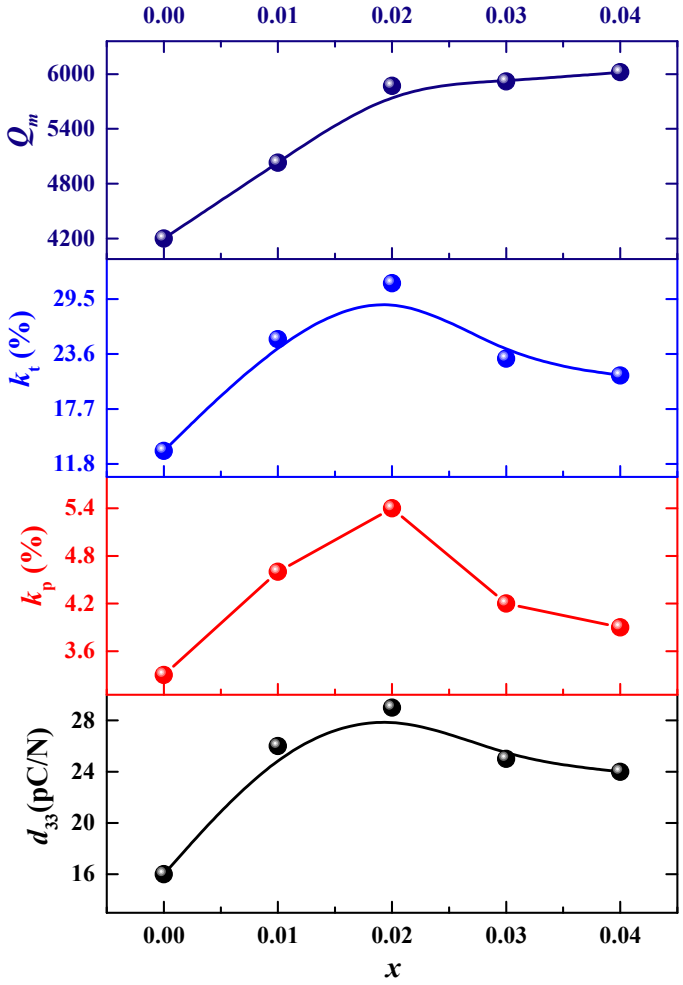

Figure 7. Room temperature electrical properties of the Mn/Nb co-doped NBT.

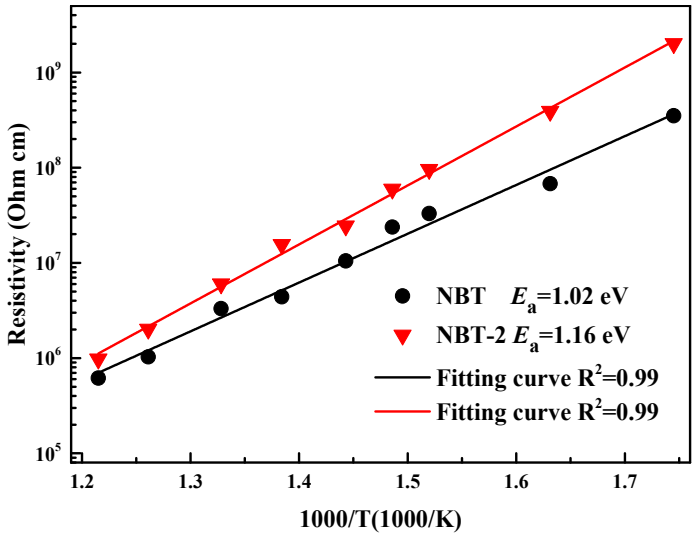

Figure 8. Temperature dependence of DC resistivity of the NBT and NBT-2 ceramics.

The effect of thermal annealing on the piezoelectric coefficient d_{33} of the NBT and NBT-2 ceramics has been investigated and shown in Figure 9, and the inset of Figure 9 gives

the relative d_{33} as a function of the annealing temperature. It can be seen that the value of d_{33} remains unchanged until 400 °C and begins to sharply drop after 500 °C, indicating good thermal stability. In addition, from the insert, it can be seen that the relative d_{33} of the NBT-2 ceramics decreases slowly and is lower than that of the pure NBT ceramics, demonstrating the enhanced thermal stability of the NBT-2 ceramics. This can be explained as follows. As known, the internal stresses induced during the annealing process led to the depolarization of piezoelectric ceramics. The introduction of Mn/Nb compound ions into the B-site of the NBT ceramics, which causes the lattice distortion, will decrease the internal stresses and result in the enhanced thermal stability of NBT-2 ceramics.

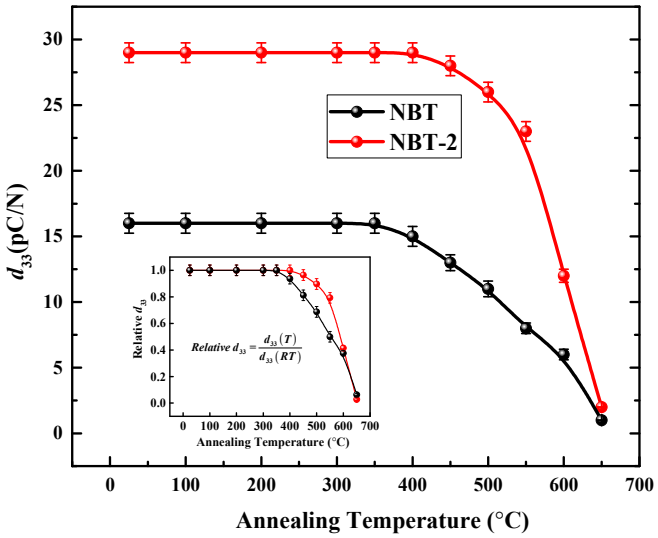

Figure 9. Effect of the thermal annealing on the piezoelectric coefficient d_{33} of the NBT and NBT-2 piezoelectric ceramics.

4. Conclusions

In this paper, series of the *B*-site Mn/Nb co-doped NBT-100*x* ceramics with typical bismuth oxide layer type phase structure and high anisotropic plate-like morphology were prepared and investigated in detail using conventional solid-state reaction method. The multi ions of Mn^{2+} and Nb^{5+} enter the *B*-site of the NBT ceramics and replace the Ti^{4+} with the equal type of $(Mn_{1/3}Nb_{2/3})^{4+}$, resulting in crystal lattice distortion with enlarged lattice parameters. The SEM images exhibit the high anisotropy and plate-like morphology of the Mn/Nb co-doped NBT ceramics, and the grain size can be found to be obviously enlarged with the increasing Mn/Nb co-doped content. The dielectric permittivity increases from 145 to 160, and the dielectric loss tan δ reduced, especially at 1MHz. The maximum of the d_{33} was found to be 29 pC/N for the NBT-2 ceramics, nearly twice that of the unmodified NBT ceramics. The highest values of planar electromechanical coupling k_p and the thickness coupling factor k_t were also obtained for the NBT-2 ceramics, at 5.4% and 31.2%, respectively. The Curie temperature T_c is sensitive to the Mn/Nb co-doped contents and linearly increases from 646 °C to 660 °C with the increasing doping level *x*. The enhanced resistivity of 10^6 Ω·cm at 500 °C and activation energy of 1.16 eV of Mn/Nb co-doped may be attributed to the restriction on the movements of the oxygen vacancies. All the results together with the good thermal stability demonstrate the potentials of the Mn/Nb co-doped NBT-100*x* ceramics for high temperature piezoelectric applications and the Mn/Nb co-doping as an effective method to improve the electrical performance of NBT based piezoelectric ceramics, which can be further extended to other BLSFs type high temperature piezoelectric ceramic systems.

Author Contributions: Conceptualization, T.Z., C.F. and Y.Q.; methodology, T.Z., K.S., X.S. and Y.Q.; software, T.Z.; validation, T.Z. and J.Z.; formal analysis, T.Z.; investigation, T.Z.; resources, T.Z. and

J.Z.; data curation, T.Z.; writing—original draft preparation, T.Z.; writing—review and editing, T.Z., C.F. and Y.Q.; visualization, T.Z. and W.L.; supervision, C.F., Y.Q. and X.D.; project administration, C.F., Y.Q. and X.D.; funding acquisition, T.Z., C.F. and Y.Q.; All authors have read and agreed to the published version of the manuscript.

Funding: This work was supported by the Fundamental Research Funds for the Central Universities under Grant ZYTS23029; the State Key Laboratory of Crystal Materials at Shandong University under Grant KF2211; the China Postdoctoral Science Foundation under Grant 2019M663927XB; the Cooperation Program of XDU-Chongqing IC Innovation Research Institute under Grant CQIRI-2022CXY-Z07; the National Natural Science Foundation of China under Grant 51802242; and the National Natural Science Foundation of Shaanxi Province under Grants 2019JQ-313, 2020JM-205, and 2020JM-253.

Data Availability Statement: The data used to support the findings of this study are available from the corresponding author upon request.

Conflicts of Interest: The authors declare no conflict of interest.

References

1. Jaffe, B. *Piezoeletric Ceramics*; Academic: London, UK, 1971.
2. Ferreira, P.M.; Machado, M.A.; Carvalho, M.S.; Vidal, C. Embedded Sensors for Structural Health Monitoring: Methodologies and Applications Review. *Sensors* **2022**, *22*, 8320. [CrossRef] [PubMed]
3. Ai, D.; Luo, H.; Zhu, H. Numerical and experimental investigation of flexural performance on pre-stressed concrete structures using electromechanical admittance. *Mech. Syst. Signal Process.* **2019**, *128*, 244–265. [CrossRef]
4. Voutetaki, M.E.; Naoum, M.C.; Papadopoulos, N.A.; Chalioris, C.E. Cracking Diagnosis in Fiber-Reinforced Concrete with Synthetic Fibers Using Piezoelectric Transducers. *Fibers* **2022**, *10*, 5. [CrossRef]
5. Zhang, S.; Yu, F.; Green, D.J. Piezoelectric Materials for High Temperature Sensors. *J. Am. Ceram. Soc.* **2011**, *94*, 3153–3170. [CrossRef]
6. Wu, J.; Gao, X.; Chen, J.; Wang, C.-M.; Zhang, S.; Dong, S. Review of high temperature piezoelectric materials, devices, and applications. *Acta Phys. Sin.* **2018**, *67*, 207701. [CrossRef]
7. Kazys, R.; Vaskeliene, V. High Temperature Ultrasonic Transducers: A Review. *Sensors* **2021**, *21*, 3200. [CrossRef]
8. Wang, Q.; Wang, C.M.; Wang, J.F.; Zhang, S.J. High performance Aurivillius-type bismuth titanate niobate (Bi_3TiNbO_9) piezoelectric ceramics for high temperature applications. *Ceram. Int.* **2016**, *42*, 6993–7000. [CrossRef]
9. Cao, Z.P.; Wang, C.M.; Zhao, T.L.; Yu, S.L.; Wu, H.Z.; Wang, Y.M.; Wang, Q.; Liang, Y.; Wei, Y.N.; Zhang, Y.; et al. Piezoelectric properties and thermal stabilities of strontium bismuth titanate ($SrBi_4Ti_4O_{15}$). *Ceram. Int.* **2015**, *41*, 13974–13982. [CrossRef]
10. Wang, H.; Jiang, X.; Chen, C.; Huang, X.; Nie, X.; Yang, L.; Fan, W.; Jie, S.; Wang, H. Structure and electrical properties of Ce-modified $Ca_{1-x}Ce_xBi_2Nb_{1.75}(Cu_{0.25}W_{0.75})_{0.25}O_9$ high Curie point piezoelectric ceramics. *Ceram. Int.* **2022**, *48*, 1723–1730. [CrossRef]
11. Aurivillius, B. Mixed Bismuth Oxides with Layer Lattices. 1. the Structure Type of $CaNb_2Bi_2O_9$. *Ark. Kemi* **1949**, *1*, 463–480.
12. Aurivillius, B. Mixed Oxides with Layer Lattices. 3. Structure of $BaBi_4Ti_4O_{15}$. *Ark. Kemi* **1950**, *2*, 519–527.
13. Xie, X.; Zhou, Z.; Chen, T.; Liang, R.; Dong, X. Enhanced electrical properties of NaBi modified $CaBi_2Nb_2O_9$-based Aurivillius piezoceramics via structural distortion. *Ceram. Int.* **2019**, *45*, 5425–5430. [CrossRef]
14. Rehman, F.; Li, J.-B.; Saeed, Y.; Ahmad, P. Dielectric behaviors and electrical properties of Gd-doped Aurivillius $KBi_4Ti_4O_{15}$ ceramics. *J. Mater. Sci.-Mater. Electron.* **2020**, *31*, 14674–14680. [CrossRef]
15. Wu, W.; Han, Y.; Huang, X.; Du, J.; Bai, W.; Wen, F.; Wu, W.; Zheng, P.; Zheng, L.; Zhang, Y. Electrical properties of a Cr_2O_3-modified $Na_{0.5}Bi_{4.5}Ti_4O_{15}$-$Na_{0.5}Bi_{0.5}TiO_3$ composite ceramic. *J. Aust. Ceram. Soc.* **2021**, *57*, 321–326. [CrossRef]
16. Chen, J.-N.; Wang, Q.; Lu, H.-T.; Zhao, X.; Wang, C.-M. Enhanced electrical properties and conduction mechanism of A-site rare-earth Nd-substituted $CaBi_2Nb_2O_9$. *J. Phys. D-Appl. Phys.* **2022**, *55*, 315301. [CrossRef]
17. Chen, N.; Wang, F.; Li, X.; Xie, Y.; Xi, J.; Guan, S.; Shi, W.; Chen, H.; Xing, J.; Zhu, J. Improving the piezoelectric properties of CBN-based ceramic by a Ce ion. *J. Am. Ceram. Soc.* **2022**, *105*, 6207–6216. [CrossRef]
18. Zhang, Y.; Liang, R.; Zhou, Z. Enhanced electrical properties of Cr_2O_3 addition NBT-based high-temperature piezoelectric ceramics. *J. Am. Ceram. Soc.* **2023**, *106*, 2357–2365. [CrossRef]
19. Zulhadjri; Wendari, T.P.; Mawardi, F.; Putri, Y.E.; Septiani, U. Effect of Gd^{3+}/Ti^{4+} heterovalent substitution on the crystal structure, morphology, optical properties, and phase transition behavior of bismuth layer-structured $SrBi_2Nb_2O_9$. *J. Solid State Chem.* **2023**, *319*, 123774. [CrossRef]
20. Shen, Z.-Y.; Sun, H.; Tang, Y.; Li, Y.; Zhang, S. Enhanced piezoelectric properties of Nb and Mn co-doped $CaBi_4Ti_4O_{15}$ high temperature piezoceramics. *Mater. Res. Bull.* **2015**, *63*, 129–133. [CrossRef]
21. Liu, Y.; Zhang, Y.; Zhu, L.; Zheng, P.; Bai, W.; Li, L.; Wen, F.; Xu, Z.; Zheng, L.; Zhang, Y. Enhanced piezoelectric activity with good thermal stability and improved electrical resistivity in Ta-Mn co-doped $CaBi_4Ti_4O_{15}$ high-temperature piezoceramics. *Ceram. Int.* **2020**, *46*, 22532–22538. [CrossRef]

22. Zhang, F.; Shi, W.; Guan, S.; Xu, Y.; Yang, H.; Chen, H.; Xing, J.; Liu, H.; Chen, Q. Enhanced electrical properties and thermal stability of W/Cr co-doped BIT-based high-temperature piezoelectric ceramics. *J. Alloys Compd.* **2022**, *907*, 164492. [CrossRef]
23. Qin, L.; Jiang, C.; Liu, K.; Chen, Y.; Du, Y.; Zuo, Y.; Chen, Y.; Cao, W. Structural and electric properties of Ce-doped $Na_{0.5}Bi_{4.5}Ti_4O_{15}$ piezoceramics with high Curie temperatures. *J. Am. Ceram. Soc.* **2020**, *103*, 4083–4089. [CrossRef]
24. IEEE. IEEE Standard on Piezoelectricity. *IEEE Trans. Ultrason. Ferroelectr. Freq. Control.* **1996**, *43*, 717.
25. Zhao, T.-L.; Guo, Z.-L.; Wang, C.-M. The Effects of Na/K Ratio on the Electrical Properties of Sodium-Potassium Bismuth Titanate $Na_{0.5}Bi_{4.5}Ti_4O_{15}$-$K_{0.5}Bi_{4.5}Ti_4O_{15}$. *J. Am. Ceram. Soc.* **2012**, *95*, 1062–1067. [CrossRef]
26. Shannon, R.D.; Prewitt, C.T. Effective ionic radii in oxides and fluorides. *Acta Cryst. B* **1969**, *25*, 925–946. [CrossRef]
27. Chamberland, B. The major ternary structural families: O. Muller and R. Roy. Springer, Berlin, 1974, 487 pp., D.M. *Int. J. Miner. Process.* **1975**, *2*, 368. [CrossRef]
28. Zuo, Y.; Fang, Z.; Fan, D.; Liu, K.; Niu, H.; Wang, H.; Du, Y.; Shen, M.; Shang, X.; Li, Z.; et al. Interrelation between lattice structures and polarization in high Curie temperature piezoelectric $Na_{0.5}Bi_{4.46}Ce_{0.04}Ti_{4-x}Co_xO_y$ ceramics. *Ceram. Int.* **2022**, *48*, 9297–9303. [CrossRef]
29. Zhang, Y.; Ke, X.; Zhao, K.; Zhou, Z.; Liang, R. Ca^{2+} doping effects on the structural and electrical properties of $Na_{0.5}Bi_{4.5}Ti_4O_{15}$ piezoceramics. *Ceram. Int.* **2022**, *48*, 31265–31272. [CrossRef]
30. Tang, Y.; Shen, Z.-Y.; Du, Q.; Zhao, X.; Wang, F.; Qin, X.; Wang, T.; Shi, W.; Sun, D.; Zhou, Z.; et al. Enhanced pyroelectric and piezoelectric responses in W/Mn-codoped $Bi_4Ti_3O_{12}$ Aurivillius ceramics. *J. Eur. Ceram. Soc.* **2018**, *38*, 5348–5353. [CrossRef]
31. Zhang, X.; Jiang, G.; Guo, F.; Liu, D.; Zhang, S.; Yang, B.; Cao, W. Mn doping effects on electric properties of $0.93(Bi_{0.5}Na_{0.5})TiO_3$-$0.07Ba(Ti_{0.945}Zr_{0.055})O_3$ ceramics. *J. Am. Ceram. Soc.* **2018**, *101*, 2996–3004. [CrossRef]